Euro. Jnl of Applied Mathematics (2003), *vol.* 14, *pp.* 407–420.
DOI: 10.1017/S0956792503005187 Printed in the United Kingdom

Singular Hopf bifurcation to strongly pulsating oscillations in lasers containing a saturable absorber

GREGORY KOZYREFF† and THOMAS ERNEUX

Optique Nonlinéaire Théorique, Université Libre de Bruxelles, Campus Plaine, C.P. 231, 1050 Bruxelles, Belgium

(*Received 5 July 2001; revised 19 September 2002*)

The equations describing the pulsating output of a laser containing a saturable absorber are investigated numerically and analytically. The laser admits a singular Hopf bifurcation to a nearly vertical branch of periodic solutions. Using asymptotic methods, we determine a simplified problem that describes the transition from harmonic to pulsating oscillations as the bifurcation parameter is changed. This transition occurs in a layer bounded by the Hopf bifurcation point, and by a critical point near which the branch of solutions becomes vertical.

1 Introduction

Lasers containing a Saturable Absorber (LSA) are known to produce short and intense pulses of laser light [18, 20, 22, 28]. They are of practical interest for many applications that request extremely short ($<$1 ns) high-peak-power ($>$10 kW) pulses of light. The short pulse widths are useful for high-precision optical ranging with applications in automated production. The high peak output intensities are needed for efficient nonlinear frequency generation or ionization of materials, with applications in microsurgery and ionization spectroscopy. The laser intensity pulses can be simulated numerically by using the laser rate equations. They consist of one equation for the laser field in the cavity and two equations for the gain and nonlinear losses. Comparative experimental and numerical studies have been first proposed for CO_2 LSAs [2, 3, 25, 26]. They showed that the laser pulsating output corresponds to a limit-cycle solution which emerges from a homoclinic bifurcation [9, 10]. More recently, the pulsating output of microchip solid state LSAs as well as semiconductor LSAs have been investigated in the laboratories. Microchip lasers are small, easy to manipulate and offer high performances for the pulse width and/or peak-power [23, 30, 31]. Semiconductor lasers exhibit high repetition rates which ranges from hundred of megahertz to a few gigahertz [1, 16]. They are interesting for telecommunication and for optical data storage using Compact Disc (CD) or Digital Versatile Disc (DVD) systems [14, 15, 17, 21, 24, 27, 29]. Previous work has focused on laser systems such as the CO_2 laser, where gain and nonlinear losses are characterized by quite similar decay rates. A complete codimension-two analysis corresponding to that limiting case was

† Current address: OCIAM, Mathematical Institute, 24–29 St Giles', Oxford OX1 3LB, UK.

carried out in Dubbeldam & Krauskopf [9]. The situation is different, however, with the solid state microchip laser subject to a semiconductor saturable absorber. While these laser systems are still described by the same rate equations, they exhibit markedly different ranges of parameter values [8, 11]. The strongly pulsating oscillations now correspond to a limit-cycle that emerges from a Hopf bifurcation point rather than from a homoclinic bifurcation. As the bifurcation parameter is progressively increased, the branch of periodic solutions is parabolic in the near vicinity of the bifurcation point, then becomes almost vertical, and finally saturates at a fixed amplitude.

The main objective of this paper is to study this Hopf bifurcation. Of particular physical interest is the size of the Hopf bifurcation layer, which is proportional to a small parameter in the laser equations. This parameter is defined as the ratio of two time scales. Because the size of the Hopf bifurcation layer decreases to zero as this parameter moves to zero, the Hopf bifurcation problem is a singular perturbation problem.

Singular Hopf bifurcations typically occur in systems of nonlinear ordinary differential equations exhibiting fast and slow variables i.e. as some of the derivatives are multiplied by a small parameter. They have been studied for two variable systems of the form

$$x' = f(x, y, \lambda), \tag{1.1}$$

$$y' = \varepsilon g(x, y, \lambda) \tag{1.2}$$

modelling mechanical, electronic, or biochemical oscillators [13]. In (1.1) and (1.2), ε is a small parameter that measures the slow decay rate of y compared to the decay of x; λ is defined as the deviation of a bifurcation parameter from its Hopf value at $\varepsilon = 0$. Singular perturbation methods have been used to derive a normal form for these equations which are valid close to the zero solution $x = y = 0$ [4]–[6]. After rescaling time and the dependent variables, the reduced equations are given by

$$\dot{u} = v + u^2/2 + O\left(\varepsilon^{1/2}\right), \tag{1.3}$$

$$\dot{v} = -u + O\left(\varepsilon^{1/2}\right). \tag{1.4}$$

These equations hold provided that the partial derivatives of f and g satisfy $f_x = 0$, $f_y g_x < 0$, and $f_{xx} \neq 0$ at $x = y = \lambda = 0$. The leading problem is conservative and requires a higher-order analysis in order to determine the amplitude of the periodic solutions [4, 5]. The derivation of (1.3) and (1.4) has been reviewed and extended to higher-dimensional systems by Braaksma [7].

More recently, we have examined a laser Hopf bifurcation problem exhibiting slow-fast limit-cycle dynamics and formulated by the following two-variable equations [12]:

$$x' = f(x, y, \lambda, \varepsilon), \tag{1.5}$$

$$y' = \varepsilon g(x, y, \lambda, \varepsilon). \tag{1.6}$$

Here the small parameter ε multiplies g, but also appears in the nonlinear functions f and g, causing the presence of a saddle-point in a close vicinity of the unstable focus. A normal form can be obtained but is different from (1.3) and (1.4). It is given by

$$\dot{u} = (1 + u)\, v + O(\varepsilon), \tag{1.7}$$

$$\dot{v} = -u\,(\kappa - v) + O(\varepsilon), \tag{1.8}$$

https://doi.org/10.1017/S0956792503005187 Published online by Cambridge University Press

where $\kappa > 0$. The leading problem is conservative and a higher order analysis is again needed in order to find the periodic solutions. Both for (1.1)–(1.2) and (1.5)–(1.6), the bifurcation diagram of the reduced problems shows the gradual change of the periodic solution from harmonic to pulsating oscillations. The amplitude of the oscillations becomes unbounded at a critical value $\lambda = \lambda_c$. The point $|\lambda_c| = O(\varepsilon)$ can be determined analytically and defines the size of the Hopf bifurcation layer.

Three variable systems exhibiting one fast and *two* slow variables of the form

$$x' = f(x, y, z, \lambda), \tag{1.9}$$

$$y' = \varepsilon g(x, y, z, \lambda), \tag{1.10}$$

$$z' = \varepsilon h(x, y, z, \lambda) \tag{1.11}$$

describe the pulsating oscillations of lasers containing a saturable absorber but are harder to analyze. As we shall demonstrate for our specific problem, the local analysis of the Hopf transition leads to a simpler three-variable problem. The reduced problem is no more conservative and the periodic solutions cannot be constructed analytically. Nevertheless, the simplicity of the reduced three-variable equations allows us to determine analytically the size of the Hopf layer.

The paper is organized as follows. In § 2, we formulate the laser equations, introduce the Hopf bifurcation point and show a typical bifurcation diagram of the periodic solutions. The Hopf nearly vertical branch of solutions is investigated in § 3 by deriving simplified equations. In § 4, the bifurcation diagram is further studied analytically by examining another limit of the parameters. Finally, we discuss in § 5 the physical and mathematical significance of our results.

2 Formulation and Hopf bifurcation

In a Laser with a Saturable Absorber (LSA), two spatially separated cells are placed in the laser cavity. The role of the two cells is quite different. One of them is an active or amplifying medium. It consists of atoms with a positive population inversion, achieved by means of an external pump. The second cell is a passive, or absorbing medium. It is left with a negative population inversion. Since the atomic systems are separated, they will interact only via the field in the cavity. The simplest semiclassical model of a LSA considers two homogeneously broadened (two levels) atomic systems. These atoms are assumed to interact only with one cavity mode. Furthermore, the radiation is tuned with the transition frequencies of both systems which are assumed equals. This leads to the following three equations for the intensity of the laser field I, and the population inversions N and $\overline{N}$ for the active and passive media [18, 20, 22, 28]:

$$I' = I(-1 + N + \overline{N}), \tag{2.1}$$

$$N' = \gamma(A - N - NI), \tag{2.2}$$

$$\overline{N}' = \overline{\gamma}(-\overline{A} - \overline{N}(1 + \alpha I)). \tag{2.3}$$

In these equations, A and $\overline{A}$ are the pump parameters of the amplifying and absorbing media, respectively. The parameter α represents the relative saturability of the absorber

https://doi.org/10.1017/S0956792503005187 Published online by Cambridge University Press

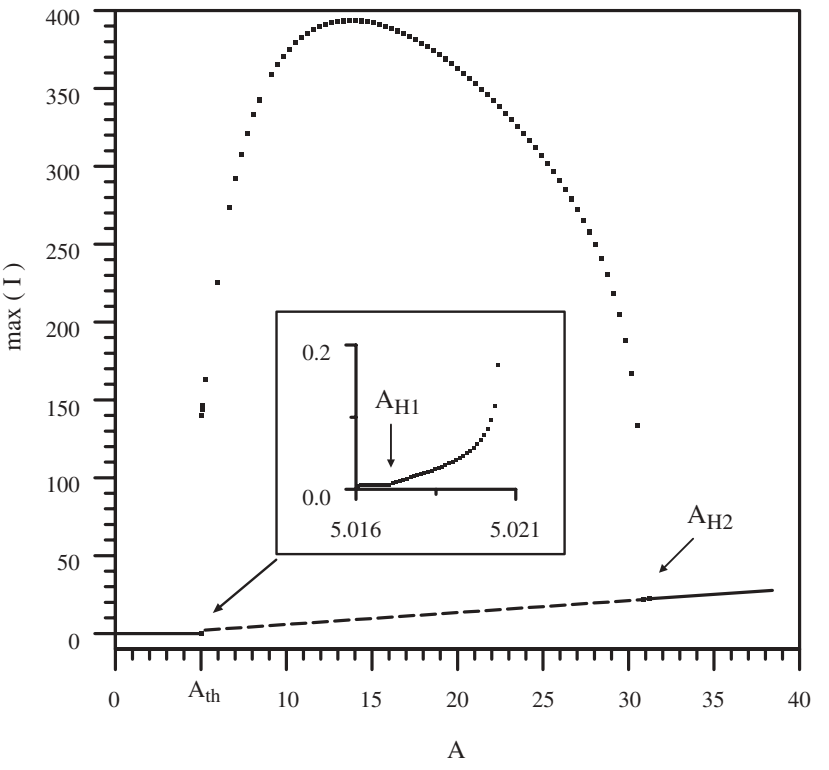

FIGURE 1. Bifurcation diagram of the laser equations (2.1)–(2.3). The maximum intensity is represented as a function of A. The values of the fixed parameters are $\gamma = 10^{-2}$, $\overline{\gamma} = 10^{-1}$, $\overline{A} = 4$ and $\alpha = 0.5$. The branch of steady state solutions emerges at $A = A_{th} = 5$ and its intensity changes linearly with A as given by (2.5). Full and broken lines correspond to stable and unstable steady states, respectively. The branch of periodic solutions connects the two Hopf bifurcation points A_{H1} and A_{H2}. A_{H1} is slightly larger than $A = A_{th}$. The inset in the figure details the Hopf bifurcation layer and shows that the branch becomes vertical near $A = 5.02$. We note that this value matches the value predicted by the asymptotic analysis, i.e. $A^* \simeq A_{th} + \gamma a^*$ where a^* is defined by (3.11).

with respect to the amplifying medium. Estimation of the dimensionless parameters [8, 11] indicates that γ and $\overline{\gamma}$ are small parameters for all type of lasers ($\gamma = O(10^{-3} - 10^{-7})$) and that α and $\overline{A}$ are generally larger than one (except for microchip lasers [11]). The control parameter A is assumed larger than the laser first threshold $A = A_{th}$ defined by

$$A_{th} \equiv 1 + \overline{A}. \tag{2.4}$$

A typical bifurcation diagram of the steady and periodic solutions is shown in Figure 1. As A is increased, the zero intensity solutions looses its stability at $A = A_{th}$. A non zero intensity steady state emerges from this point and is given by

$$I \simeq \frac{A - A_{th}}{A_{th} - \alpha\overline{A}}. \tag{2.5}$$

for A close to A_{th}. If α is sufficiently small, $A_{th} - \alpha\overline{A}$ is positive and the bifurcation is supercritical and stable. We concentrate on this case.

https://doi.org/10.1017/S0956792503005187 Published online by Cambridge University Press

As A is further increased, the stable steady state solution (2.5) undergoes a Hopf bifurcation at a critical intensity $I = I_H$. From the linear stability analysis, we determine conditions for $I = I_H$ and the frequency of the oscillations $\omega = \omega_H$ at the Hopf bifurcation point. Assuming $I_H = O(\gamma)$ and

$$b = \overline{\gamma}/\gamma = O(1), \tag{2.6}$$

we find the approximations

$$I_H \simeq \gamma \frac{b(1+b)}{b^2\overline{A}\alpha - A_{th}} \tag{2.7}$$

and

$$\omega_H \simeq \gamma \sqrt{\frac{b^2(A_{th} - \overline{A}\alpha)}{b^2\overline{A}\alpha - A_{th}}}, \tag{2.8}$$

provided that

$$b^2\overline{A}\alpha - A_{th} > 0 \quad \text{and} \quad A_{th} - \overline{A}\alpha > 0. \tag{2.9}$$

The first condition guarantees a positive intensity at the Hopf bifurcation point. The second condition implies that the steady state bifurcation is supercritical. Equivalently, (2.9) imply conditions on the values of α and b given by

$$\frac{A_{th}}{\overline{A}b^2} < \alpha < \frac{A_{th}}{\overline{A}} \quad \text{and} \quad b > 1. \tag{2.10}$$

Knowing I_H, we may determine $A = A_H$ using (2.5) and N_H, $\overline{N}_H$ from the steady state equations. We obtain

$$A_H \simeq A_{th} + (A_{th} - \alpha\overline{A})I_H, \tag{2.11}$$

$$N_H \simeq A_{th} - \alpha\overline{A}I_H \quad \text{and} \quad \overline{N}_H \simeq -\overline{A} + \overline{A}\alpha I_H. \tag{2.12}$$

These expressions will become useful as we investigate the Hopf bifurcation problem in the next section.

As soon as A surpasses A_H (A_{H1} in Figure 1), a nearly vertical branch appears. As the branch starts to fold, the oscillations are already strongly pulsating. The branch then progressively saturates and terminates at a higher intensity Hopf bifurcation point (A_{H2} in Figure 1). In Figure 2, we show the pulsating intensities as well as the limit-cycle in the phase plane (N, I). The limit-cycle consists of a long interpulse period where I is almost zero and N is gradually increasing. This evolution is followed by a quick orbit in the phase plane which is characterized by a large intensity. Matched asymptotic methods can be used to construct the solution [10]. However, they fail to describe the Hopf bifurcation layer near the Hopf point.

3 The solution near the Hopf bifurcation point

Our objective is to determine the change from harmonic to pulsating oscillations which appears near the Hopf bifurcation point.The coordinates of the Hopf bifurcation point

https://doi.org/10.1017/S0956792503005187 Published online by Cambridge University Press

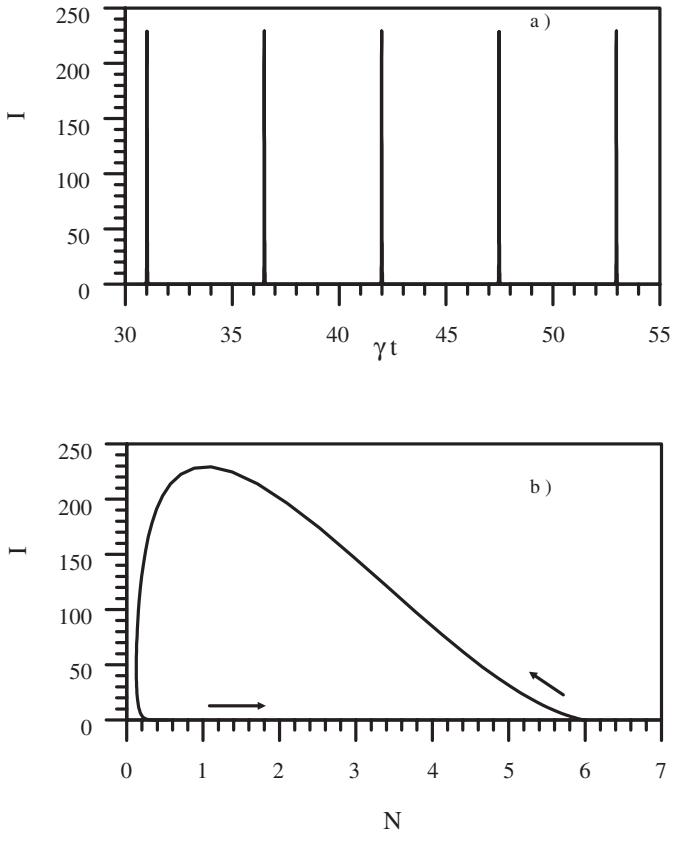

FIGURE 2. Strongly pulsating limit-cycle solution. The values of the parameters are the same as in Figure 1 and $A = 6$. (a) The intensity exhibits short and intense pulses separated by long intervals where it is nearly zero. (b) The limit-cycle orbit in the phase plane (N, I) consists of a slow regime where $I \simeq 0$ and N is gradually increasing followed by high intensity orbit where N is quickly decreasing.

(2.7), (2.8), (2.11) and (2.12) exhibit scalings with respect to γ and motivates new variables and a new bifurcation parameter. Specifically, we introduce the variables s, i, n and $\overline{n}$ defined by

$$s \equiv \gamma t, \quad i \equiv \gamma^{-1} I, \quad n \equiv \gamma^{-1}(N - A_{th}), \quad \overline{n} \equiv \gamma^{-1}(\overline{N} + \overline{A}) \tag{3.1}$$

and the parameter a given by

$$a \equiv \gamma^{-1}(A - A_{th}) \tag{3.2}$$

and rewrite (2.1)–(2.3) in terms of i, n, $\overline{n}$. Taking then the limit $\gamma \to 0$, we obtain the following equations for i, n and $\overline{n}$:

$$i' = i(n + \overline{n}), \tag{3.3}$$

$$n' = a - n - A_{th} i, \tag{3.4}$$

$$\overline{n}' = b(-\overline{n} + \overline{A}\alpha i). \tag{3.5}$$

https://doi.org/10.1017/S0956792503005187 Published online by Cambridge University Press

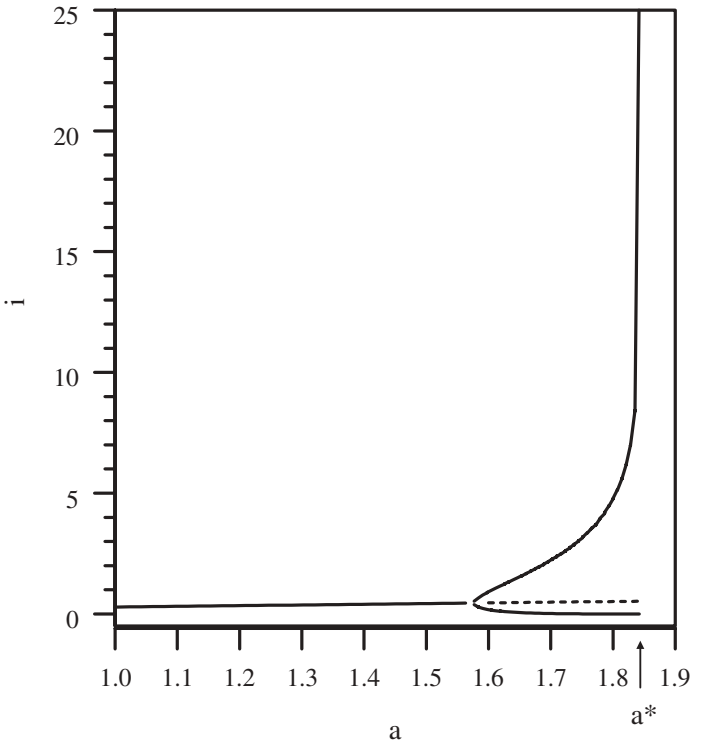

FIGURE 3. Bifurcation diagram of the reduced problem (3.3)–(3.5). The values of the parameters are $b = 10$, $\overline{A} = 5$ and $\alpha = 0.5$. The figure represents the maximum and the minimum of i as a function of $a = \gamma^{-1}(A - A_{th})$. The critical value $a = a^* \simeq 1.8421053$ where the limit-cycle orbit approaches the separatrices of the saddle is determined from (3.11). The point with the largest maximum intensity corresponds to $a = 1.8421$. If $a > a^*$, the solution of (3.3)–(3.5) is unbounded in time. The small amplitude straight line is the steady state (2.5) with $A - A_{th} = \gamma a$.

These equations are simpler than (2.1)–(2.3) because the two last equations are linear. We first verify that (3.3)–(3.5) admits the same Hopf bifurcation point as the original equations. From (3.3)–(3.5), we find that the coordinates of the Hopf bifurcation point are given by

$$\begin{aligned} i_H &= \frac{b(1+b)}{b^2\overline{A}\alpha - A_{th}}, \quad n_H = -\alpha\overline{A}i_H, \\ \overline{n}_H &= \overline{A}\alpha I_H, \quad a_H = (A_{th} - \alpha\overline{A})i_H. \end{aligned} \tag{3.6}$$

The expressions (3.7) match our earlier expressions (2.7), (2.11) and (2.12). The numerical branch of periodic solutions is shown in Figure 3. We note that the branch is parabolic near the bifurcation point and then becomes vertical at a particular value of $a = a^*$. Equations (3.3)–(3.5) cannot be solved analytically. Nevertheless, as we shall now demonstrate, the point where the amplitude of the oscillations becomes unbounded can be determined analytically.

https://doi.org/10.1017/S0956792503005187 Published online by Cambridge University Press

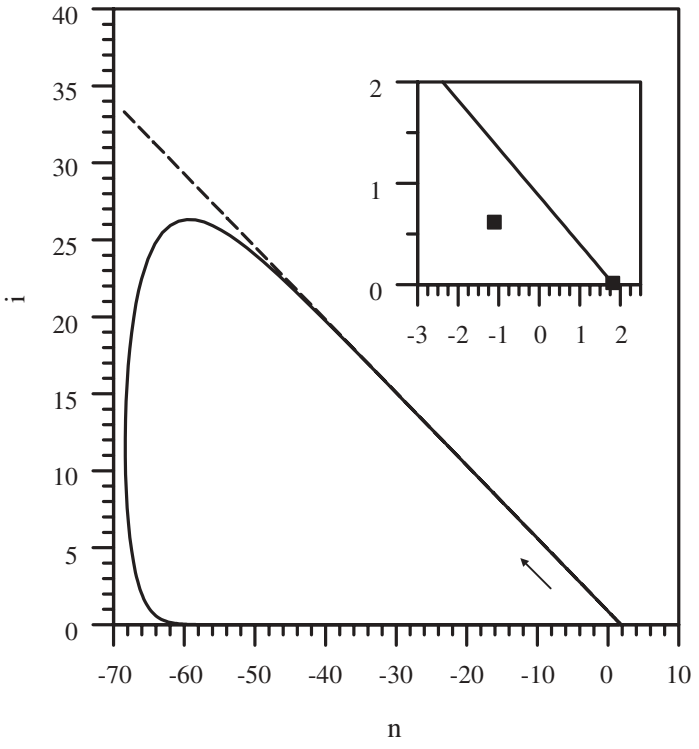

FIGURE 4. Limit-cycle solution of (3.3)–(3.5). The values of the parameters are the same as in Figure 3 and $a = 1.8421$. The dotted line is the separatrix or unstable manifold emerging from the saddle point $(i, n) = (0, a)$. The inset in the figure shows the saddle point as well as the unstable focus.

As $a - a^* \to 0^-$, we note in the phase plane (n, i) and $(\overline{n}, i)$ that part of the limit-cycle orbit is spending more and more time near the unstable separatrix that emerges from the saddle point $(i, n, \overline{n}) = (0, a, 0)$ (see Figure 4). Moreover, the trajectories $n = n(i)$ and $\overline{n} = \overline{n}(i)$ are nearly straight lines as the orbit is close to the separatrix. This suggest that at $a = a^*$, the limit-cycle degenerates into the line $i = 0$ and the line $n = n(i)$ and $\overline{n} = \overline{n}(i)$ that varies linearly with i. We verify this hypothesis by writing equations for dn/di and $d\overline{n}/di$. From (3.3)–(3.5), we obtain

$$\frac{dn}{di} = \frac{a - n - A_{th} i}{i(n + \overline{n})}, \tag{3.7}$$

$$\frac{d\overline{n}}{di} = \frac{b(-\overline{n} + \overline{A}\alpha i)}{i(n + \overline{n})}. \tag{3.8}$$

We then seek a solution of the form

$$n = a + \beta i \quad \text{and} \quad \overline{n} = \delta i \tag{3.9}$$

where β and δ are unknown coefficients to be determined. Substituting (3.9) into (3.7)

https://doi.org/10.1017/S0956792503005187 Published online by Cambridge University Press

and (3.8) gives the following conditions for β, δ and a:

$$\beta = -\delta = \frac{-A_{th}}{1+a} \tag{3.10}$$

and

$$a = a^* = \frac{b(A_{th} - \overline{A}\alpha)}{b\overline{A}\alpha - A_{th}}. \tag{3.11}$$

Using (3.11), the numerical value of a^* is shown in Figure 3. The size of the Hopf bifurcation layer is given by $a^* - a_H$. Using (3.7) and (3.11), we find that

$$a^* - a_H = \frac{b^2(A_{th} - \overline{A}\alpha)^2}{(b\overline{A}\alpha - A_{th})(b^2\overline{A}\alpha - A_{th})}. \tag{3.12}$$

We briefly discuss the expression (3.12). First, we note that $a^* - a_H$ is proportional to b^{-1} for large b. This means that the Hopf bifurcation branch becomes more and more vertical as we increase b. We comment on the large-b limit in the next section. Secondly, $a^* - a_H$ may become large if the denominator is sufficiently small. Decreasing α progressively from $\alpha = 1$ and remembering that $b > 1$, we see that a^* approaches infinity as $\alpha \to \alpha_c$, where

$$\alpha_c = A_{th}/(b\overline{A}). \tag{3.13}$$

Equations (3.3)–(3.5) then admit a limit-cycle solution for all $a > a_H$. However, a cannot be too large, since our analysis based on the small-γ limit also assumed $a = O(1)$.

The point where the Hopf bifurcation branch becomes vertical is estimated at $A^* \simeq 5.02$ (see the inset of Figure 1), meaning a value of $a^* \simeq 2$. From (3.11) with $b = 10$, $\overline{A} = 4$ and $\alpha = 0.5$, we determines $a^* = 2$. Thus, (3.11) gives a good analytical estimate of the Hopf bifurcation layer.

4 From harmonic to strongly pulsating oscillations

We may further progress in the analytic description of the bifurcation layer if we assume the asymptotic limit $b = \bar{\gamma}/\gamma \gg 1$. This limit applies to the Nd:YAG/Cr:YAG microchip lasers, for which $\gamma = 1.7\ 10^{-6}$, $\bar{\gamma} = 6.3\ 10^{-5}$ [30, 31] and the Nd:YVO4 microchip laser with semiconductor saturable absorber mirror (SESAM) for which $\gamma = 3.7\ 10^{-7}$, $\bar{\gamma} = 9.3\ 10^{-2}$ [23]. To exploit this particular feature of the laser equations, we rewrite (3.5) as

$$\bar{n} - \alpha\bar{A}i = -b^{-1}\bar{n}'. \tag{4.1}$$

Because b^{-1} is small, $\bar{n} = \alpha\bar{A}i + O(b^{-1})$, and substituting this answer into the right hand side of (4.1), we obtain the two-term approximation

$$\bar{n} \simeq \alpha\bar{A}i - b^{-1}\alpha\bar{A}i'. \tag{4.2}$$

With (4.2), (3.3)–(3.5) reduce to the following equations for i and n only:

$$i' = i(n + \alpha\bar{A}i) - b^{-1}\alpha\bar{A}ii', \tag{4.3}$$

$$n' = a - n - A_{th}i. \tag{4.4}$$

https://doi.org/10.1017/S0956792503005187 Published online by Cambridge University Press

The steady state solution of (4.3)–(4.4) is given by $i_S = a/(A_{th} - \alpha\bar{A})$, $n_S = -a(\alpha\bar{A})/(A_{th} - \alpha\bar{A})$ and the Hopf bifurcation is now located at $a_H = (A_{th} - \alpha\bar{A})/(\alpha\bar{A})$. This expression agrees with the limit $b^{-1} \to 0$ of (3.7). We next introduce a new bifurcation parameter a_1 defined by

$$a_1 \equiv b\frac{a - a_H}{a_H}, \tag{4.5}$$

as well as the new variables u and v given by

$$u \equiv \frac{i}{i_S} - 1, \quad v \equiv n - n_S + u. \tag{4.6}$$

The variable u and v represent deviations of the intensity i and population inversion n from their steady-state values. In terms of (4.5) and (4.6), (4.3) and (4.4) become

$$\begin{aligned} u' &= (1+u)v + b^{-1}f_u, \\ v' &= -u(a_H - v) + b^{-1}f_v, \end{aligned} \tag{4.7}$$

where

$$f_u = (1+u)(a_1 u - u'), \quad f_v = f_u - (a_H + 1)u. \tag{4.8}$$

Setting $b^{-1} = 0$ in (4.7), we obtain a conservative system which turns out to be equivalent to the Lotka-Volterra equations. It admits a one-parameter family of periodic solutions (u_0, v_0) that satisfies the first integral

$$E = u_0 - \ln(1 + u_0) - v_0 - a_H \ln(a_H - v_0) \tag{4.9}$$

where E is the constant of integration. Close to the centre $(u_0, v_0) = (0, 0)$, these periodic solutions are nearly harmonic while they become strongly pulsating for larger peak values of u_0. This reduced system is therefore able to reproduce the bifurcation layer in Figure 3. Our goal is now to determine which periodic solution (u_0, v_0) is also periodic solution of the full system (4.7) for a given value of a_1. To this end, we introduce the functional

$$\tilde{E}(u(s), v(s)) = u - \ln(1 + u) - v - a_H \ln(a_H - v). \tag{4.10}$$

This functional, computed with the true periodic solution of (4.7) should satisfy the condition

$$\int_P \tilde{E}'\, ds = 0, \tag{4.11}$$

where P is the period of the solution. Using (4.7), we can rewrite this condition as

$$b^{-1}\int_P \left\{ u(a_1 u - u') + v\left[(1+u)\frac{a_1 u - u'}{a_H - v} - \frac{a_H + 1}{a_H - v}u\right]\right\} ds = 0. \tag{4.12}$$

We now evaluate this expression with $(u, v) = (u_0, v_0)$. To this end, we note that

$$\int_P u_0 u_0'\, ds = \frac{1}{2}\left[u_0^2(s)\right]_0^P = 0. \tag{4.13}$$

https://doi.org/10.1017/S0956792503005187 Published online by Cambridge University Press

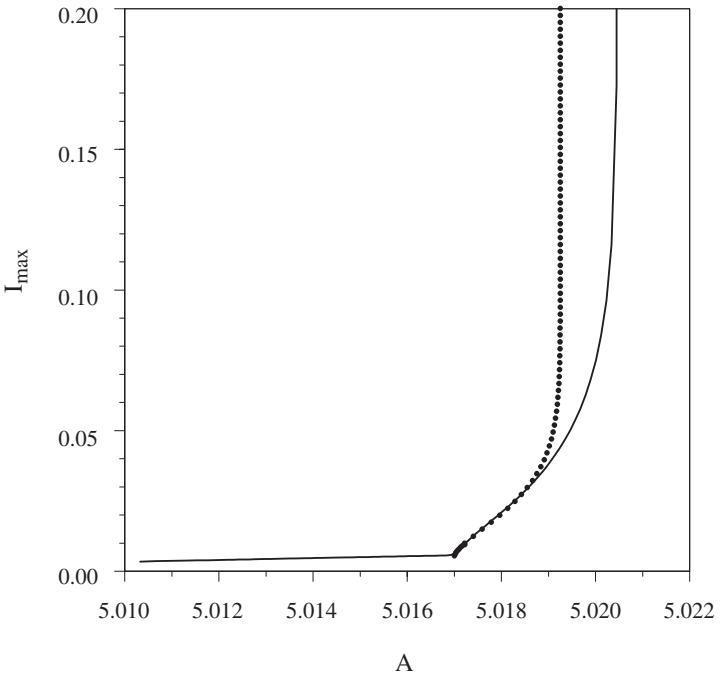

FIGURE 5. Enlargement of the bifurcation diagram in Figure 1 near the low-intensity Hopf point. The dotted line represent the analytical approximation, obtained with (4.15). The start of the analytical curve is shifted by 0.0005 on the right for a better fit with the numerical branch, which is in full line.

Moreover, using (4.7) with $b^{-1} = 0$, we find that

$$\int_P \frac{u_0 v_0}{a_H - v_0}\, ds = \int_P \frac{-v_0 v_0'}{(a_H - v_0)^2}\, ds = \left[-\ln(a_H - v_0(s)) - \frac{a_H}{a_H - v_0(s)} \right]_0^P = 0. \tag{4.14}$$

In the same way, one can show that $\int_P u_0^n v_0/(a_H - v_0)\, ds = 0$ for all positive integer n. Consequently, (4.12) reduces to the following condition

$$a_1 = \left(\int_P \frac{v_0^2 (1 + u_0)^2}{a_H - v_0}\, ds \right) \Big/ \left(\int_P u_0^2\, ds \right). \tag{4.15}$$

We may now assign a value of a_1 for each solution of the family (4.9) by computing the integrals in the right-hand side of (4.15). The resulting Hopf bifurcation branch is shown in Figure 5 and is compared, after rescaling, with the inset of Figure 1. Despite the moderately large value $b = 10$, the two branches agree quantitatively in the vicinity of the Hopf bifurcation. They only start to deviate as the amplitude of the solution starts to increase dramatically.

Although the integrals in the right-hand side of (4.15) need to be evaluated numerically, one can analytically estimate the value of a_1^* corresponding to the divergence of the bifurcation branch. Indeed, as $E \to \infty$ in (4.9), the periodic solution spend most of the time

https://doi.org/10.1017/S0956792503005187 Published online by Cambridge University Press

near the separatrix $v_0 = a_H$. This allow to simplify considerably the integrals in (4.15) leading to [19]

$$a_1^* = \lim_{E\to\infty} a_1 = \frac{A_{th}}{\bar{A}\alpha}. \tag{4.16}$$

Using then $a^* = a_H(1 + b^{-1}a_1^*)$, we find that it matches the two terms limit of (3.11) for b large.

5 Discussion

Singular Hopf bifurcation problems are problems where the Hopf bifurcation branch is forced to change from harmonic to strongly pulsating oscillations in the vicinity of the bifurcation point. The phenomenon occurs because of the presence of a small parameter in the evolution equations that controls the time scales of the solution. This is the case for problems exhibiting relaxation oscillations [4]. For two variable problems, the bifurcation problem generally reduces to the perturbation of a double zero eigenvalue and a conservative system of equations appears in the first approximation. But for three variable problems, a general asymptotic theory remains difficult because of the large variety of cases. In this paper, we concentrate on a laser that exhibits pulsating limit-cycle oscillations. Specifically, we examine the equations for a laser with a saturable absorber and investigate its nearly vertical Hopf bifurcation problem. From the original three variables equations, we determined a simplified problem given by (3.3)–(3.5). The bifurcation diagram of these equations needs to be studied numerically but the point where the limit-cycle solution becomes unbounded can be identified analytically. To further progress analytically, we studied the large-b limit of (3.3)–(3.5). In this limit, our equations reduce to the two variable Lotka-Volterra conservative equations [12]. A higher order analysis in b^{-1} then lead to the bifurcation equation (4.15) for the amplitude of the oscillations. We have investigated this bifurcation equation and found good agreement with the original laser equations.

As the maximum intensity of the limit-cycle solution becomes large (i.e. as $a \to a^*$), our local Hopf bifurcation theory becomes invalid and motivates a new analysis of the laser equations near $a = a^*$. This analysis is difficult because the periodic solution changes dramatically along the nearly vertical branch. Because the branch remains almost vertical as the amplitude increases, the point $A^* = A_{th} + \gamma a^*$ gives a good estimate of the point where the strongly pulsating oscillations of a LSA appears. Because these oscillations occur near the laser threshold $A = A_{th}$, experimental observations of the Hopf bifurcation branch will be possible only if the Hopf bifurcation layer is sufficiently large implying that α needs to be sufficiently small.

Acknowledgements

The research was supported by the US Air Force Office of Scientific Research grant AFOSR F49620-98-1-0400, the National Science Foundation grant DMS-9973203, the Fonds National de la Recherche Scientifique (Belgium) and the InterUniversity Attraction Pole program of the Belgian government.

References

[1] Agrawal, G. P. & Dutta, N. K. (1986) *Long-wavelength Semiconductor Lasers*. Van Nostrand Reinhold.

[2] Arimondo, E., Casagrande, F., Lugiato, L. A. & Glorieux, P. (1983) Repetitive passive Q-switching and bistability in lasers with saturable absorbers. *Appl. Phys.* **B30**, 57–77.

[3] Arimondo, E., Bootz, P., Glorieux, P. & Menchi, E. (1985) Pulse shape and phase diagram in the passive Q switching of CO_2 lasers. *J. OSA B*, **2**, 193–201.

[4] Baer, S. M. & Erneux, T. (1986) Singular Hopf bifurcation to relaxation oscillations. *SIAM J. Appl. Math.* **46**, 721–739.

[5] Baer, S. M. & Erneux, T. (1992) Singular Hopf bifurcation to relaxation oscillations II. *SIAM J. Appl. Math.* **52**, 1651–1664.

[6] Braaksma, B. (1992) Phantom ducks and models of excitability. *J. Dyn. Diff. Eq.* **4**, 485–513.

[7] Braaksma, B. (1998) Singular Hopf bifurcation in systems with fast and slow variables. *J. Nonlinear Sci.* **8**, 457–490.

[8] Carr, T. W. & Erneux, T. (2001) Dimensionless rate equations and simple conditions for self-pulsating in laser diodes. *IEEE J. Quantum Electr.* **37**, 1171–1177.

[9] Dubbeldam, J. L. A. & Krauskopf, B. (1999) Self pulsations of lasers with saturable absorber: dynamics and bifurcations. *Opt. Comm.* **159**, 325–358.

[10] Erneux, T. (1988) Q-switching bifurcation in a laser with a saturable absorber. *J. OSA B*, **5**, 1063–1069.

[11] Erneux, T., Peterson, P. & Gavrielides, A. (2000) The pulse shape of a passively Q-switched microchip laser. *Euro. Phys. J. D.* **10**, 423–431.

[12] Erneux, T. & Kozyreff, G. (2000) Nearly vertical Hopf bifurcation for a passively Q-swiched microchip laser. *J. Stat. Phys.* **101**, 543–552.

[13] Grasman, J. (1987) Asymptotic methods for relaxation oscillations and applications. *Appl. Math. Sci.* **63**.

[14] Jones, D. R., Rees, P., Pierce, I. & Summers, H. D. (1999) Theoretical optimization of self-pulsating 650-nm-wavelength AlGaInP laser diodes. *IEEE J. Selected Topics in Quantum Electr.* **5**, 740–744.

[15] Juang, C., Chen, M. R. & Juang, J. (1999) Nonlinear dynamics of self-pulsating laser diodes under external drive. *Opt. Lett.* **24**, 1349–1348.

[16] Kawaguchi, H. (1994) *Bistabilities and Nonlinearities in Laser Diodes*. Artech House.

[17] Kidoguchi, I., Adachi, H., Kamiyama, S., Fukuhisa, T., Mannoh, M. & Takamori, A. (1997) Low-Noise 650-nm AlGaInP visible laser diodes with a highly doped saturable absorber layer. *IEEE J. Quantum Electr.* **33**, 831–836.

[18] Khanin, Y. I. (1995) *Principles of Laser Dynamics*. Elsevier.

[19] Kozyreff, G. (2001) PhD Thesis, Université Libre de Bruxelles.

[20] Mandel, P. (1997) *Theoretical Problems in Cavity Nonlinear Optics*. Cambridge Studies in Modern Optics, Cambridge University Press.

[21] Mirasso, C. R., van Tartwijk, G. H. M., Hernández-Garcia, E., Lenstra, D., Lynch, S., Landais, P., Phelan, P., O'Gorman, J., San Miguel, M. & Elsässer, W. (1999) Self-pulsating semiconductor lasers: theory and experiment. *IEEE J. Quantum Electr.* **35**, 764–770.

[22] Siegman, A. E. (1986) *Lasers*. University Science Books.

[23] Spühler, G. J., Paschotta, R., Fluck, R., Braun, B., Moser, M., Zhang, G., Gini, E. & Keller, U. (1999) Experimentally confirmed design guidelines for passively Q-switched microchip lasers using semiconductor saturable absorbers. *J. OSA B*, **16**, 376–388.

[24] Summers, H. D. & Rees, P. (1997) Thermal limitation of self-pulsation in 650-nm AlGaInP laser diodes with an epitaxially integrated absorber. *Appl. Phys. Lett.* **71**, 2665–2667.

[25] Tachikawa, M., Tanii, K. & Shimizu, T. (1987) Comprehensive interpretation of passive Q switching and optical bistability in a CO_2 laser with an intracavity saturable absorber. *J. OSA B*, **4**, 387–395.

[26] Tachikawa, M., Tanii, K. & Shimizu, T. (1988) Laser instability and chaotic pulsation in a CO_2 laser with intracavity saturable absorber. *J. OSA B*, **5**, 1077–1082.
[27] Van Tartwijk, G. H. M. & San Miguel, M. (1996) Optical feedback on self-pulsating semiconductor lasers. *IEEE, J. Quantum Electr*. **32**, 1191–1202.
[28] Weiss, C. O. & Vilaseca, R. (1991) *Dynamics of Lasers*. VCH Weinheim (FRG).
[29] Yamada, M. (1993) A theoretical analysis of self-sustained pulsation phenomena in narrow-stripe semiconductor lasers. *IEEE J. Quantum Electr*. **29**, 1330–1336.
[30] Zayhowski, J. J. (1996) Ultraviolet generation with passively Q-switched microchip lasers. *Opt. Lett*. **21**, 588–590. (Errata: *Opt. Lett*. **21**, 1618.)
[31] Zayhowski, J. J. & Dill III, C. (1994) Diode-pumped passively Q-switched picosecond microchip lasers. *Opt. Lett*. **19**, 1427–1429.